Syntheses, Crystal Structures and Magnetic Properties of $Cr(NCNH_2)_4Cl_2$ and $Mn(NCNH_2)_4Cl_2$

Xiaojuan Tang[a], Manfred Speldrich[a], Andrei L. Tchougréeff[a,b], and Richard Dronskowski[a]

[a] Institute of Inorganic Chemistry, RTWH Aachen University, Landoltweg 1, 52056 Aachen, Germany

[b] Poncelet Laboratory, Independent University of Moscow, and Department of Chemistry, Moscow State (Lomonosov) University, Moscow, Russia

Reprint requests to Prof. Dr. Richard Dronskowski. Fax: +49-241-80-92642.
E-mail: drons@HAL9000.ac.rwth-aachen.de

Z. Naturforsch. **2012**, *67b*, 1 – 7 / DOI: 10.5560/ZNB.2012-0234
Received September 6, 2012

The two isotypic compounds $Cr(NCNH_2)_4Cl_2$ and $Mn(NCNH_2)_4Cl_2$ have been synthesized and characterized by X-ray diffraction. They crystallize in the cubic space group $Im\bar{3}m$ ($Z = 6$) with $a = 12.643(2)$ Å for $Cr(NCNH_2)_4Cl_2$ and $a = 12.821(1)$ Å for $Mn(NCNH_2)_4Cl_2$. The divalent transition metal ions are octahedrally coordinated by four H_2NCN molecules in equatorial and two chloride ions in axial positions. The magnetic susceptibility data of the four Curie-paramagnetic compounds $Cr(NCNH_2)_4Cl_2$, $Mn(NCNH_2)_4Cl_2$, $Co(NCNH_2)_4Cl_2$, and $Ni(NCNH_2)_4Cl_2$ have been analyzed in greater detail, including many-body quantum theory.

Key words: Chromium, Manganese, Cyanamide, Chloride, Crystal Structure, Magnetism

Introduction

In the course of transition metal cyanamide research, the crystal structures and magnetic properties of $Fe(NCNH_2)_4Cl_2$, $Co(NCNH_2)_4Cl_2$, $Ni(NCNH_2)_4Cl_2$, and $Cu(NCNH_2)_4Cl_2$ have already been communicated [1 – 3]. The chemical similarity of the NCN^{2-} anion with O^{2-} is obvious, and so is the one between H_2NCN and H_2O. The complete series of aquo-chloro complexes of the general form $M(OH_2)_4Cl_2$ (M = Cr, Mn, Fe, Co, Ni) [4 – 8] is already known. To close the cyanamide series, the two compounds $Cr(NCNH_2)_4Cl_2$, **1**, and $Mn(NCNH_2)_4Cl_2$, **2**, have been synthesized. Below, we report on their crystal structures and magnetic properties in more detail.

Results and Discussion

The X-ray crystal-structure analyses of **1** and **2** were performed based on single-crystal (Mn compound) and powder (Cr compound) diffraction data, respectively. The observed and calculated diffraction patterns of **1** are shown in Fig. 1. As expected, the structure is isotypic with $M(NCNH_2)_4Cl_2$ (M = Fe, Co, Ni and Cu).

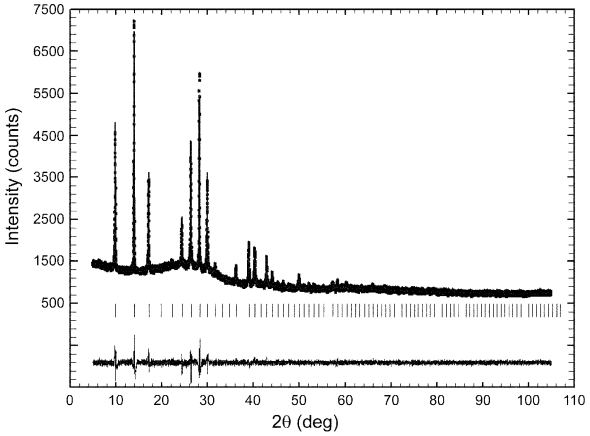

Fig. 1. Observed (circles), calculated (line), and difference (below) X-ray diffraction intensities of $Cr(NCNH_2)_4Cl_2$. The vertical markers show the positions of the Bragg reflections.

Structure

The environment of the metal atom and the crystal structure of $M(NCNH_2)_4Cl_2$ (M = Cr, **1**; Mn, **2**) are depicted in Figs. 2 and 3, respectively. Each M^{2+} ion

Table 1. Selected bond lengths (Å) and bond angles (deg) of all 3*d* transition metal tetracyanamide dichlorides, $M(NCNH_2)_4Cl_2$, with standard deviations in parentheses.

	$Cr(NCNH_2)_4Cl_2$	$Mn(NCNH_2)_4Cl_2$	$Fe(NCNH_2)_4Cl_2$ [1]	$Co(NCNH_2)_4Cl_2$ [2]	$Ni(NCNH_2)_4Cl_2$ [2]	$Cu(NCNH_2)_4Cl_2$ [3]
M–N1	$4\times2.065(9)$	$4\times2.200(3)$	$4\times212.3(4)$	$4\times2.090(3)$	$4\times2.048(3)$	$4\times2.037(4)$
M–Cl	$2\times2.745(4)$	$2\times2.5881(14)$	$2\times251.9(2)$	$2\times2.516(1)$	$2\times2.483(1)$	$2\times2.783(1)$
C–N1	1.09(2)	1.114(4)	1.125(5)	1.121(4)	1.121(4)	1.047(7)
C–N2	1.34(1)	1.336(5)	1.323(9)	1.331(5)	1.327(5)	1.343(12)
N2–H	0.91(1)	0.86(3)	0.85(4)	0.87(3)	0.93(3)	0.98(5)
M–N1–C	180	180	180	180	180	180
N1–C–N2	164.1(3)	165.4(5)	166.5(10)	166.2(5)	166.2(4)	167.4(16)
C–N2–H	113.0(6)	109.3(17)	110.9(4)	111(2)	113(2)	120(3)

is octahedrally coordinated by four nitrogen-bonded cyanamide molecules in equatorial positions and two chloride ions in axial positions. The selected bond lengths and angles of **1** and **2** are compared with those of the already reported members of the series in Table 1.

The Mn–N1 distances in **2** are 2.200(3) Å and slightly shorter than those in $Mn(NH_3)_6Cl_2$ (2.270(3) Å) [9]. The Mn–Cl distances amount to 2.5881(14) Å, somewhat longer than those in octahedral $MnCl_6$ units (2.548(2) Å) [10]. It seems that the Mn–N1 and the Mn–Cl distances agree well with the sum of the effective (high-spin) ionic radii (2.29 Å and 2.64 Å) [11].

For $Cr(NCNH_2)_4Cl_2$, **1**, the Cr–N1 and the Cr–Cl distances amount to 2.065(9) and 2.745(4) Å, respectively. On comparison with other isotypical complexes (Table 1), the Cr–N1 distance appears rather normal. The Cr–Cl distance is in very good agreement with published data such as 2.758(9) Å in $Cr(H_2O)_4Cl_2$ [4]. The somewhat larger value compared to the sum of effective (high-spin octahedral) ionic radii (2.61 Å) [11] is due to the d^4 chromium(II) ion with a high-spin electronic configuration $(t_{2g})^3(e_g)^1$. Similar findings,

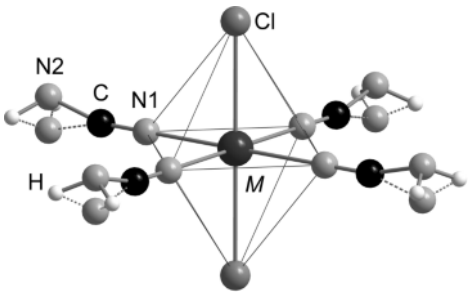

Fig. 2. The coordination environment around the M^{2+} ion (M = Cr or Mn).

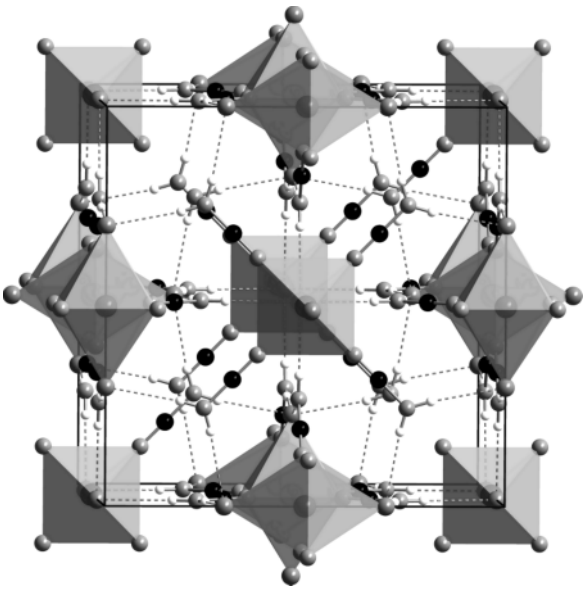

Fig. 3. Crystal structure of $M(NCNH_2)_4Cl_2$ with M = Cr or Mn; M atoms are shown in dark grey, Cl atoms in medium grey, N atoms in light grey, C atoms in black and H atoms in white.

e.g., Cr–Cl = 2.40 Å (4×) and 2.91 Å (2×), are known from $CrCl_2$ [12].

The two C–N bond lengths of the cyanamide ligands suggest a triply bonded C – N1 = 1.09(2) Å and a singly bonded C – N2 = 1.34(1) Å for **1**, as do C – N1 = 1.114(4) Å and C – N2 = 1.336(5) Å for **2**. These interatomic distances are consistent with those (1.15 and 1.31 Å) in pure molecular cyanamide (H_2NCN) [13]. While the N1–C–N2 angles are 164.1(3)° for **1** and 165.4(5)° for **2**, the N2–H bond lengths underestimated by the X-ray method are 0.91(1) Å for **1** and 0.86(3) Å for **2**. Fig. 3 indicates that each H_2NCN molecule forms two hydrogen bonds to Cl^- which functions as a four-proton acceptor. The

Cl···H distances are 2.3650(4) Å for **1** and 2.426(5) Å for **2**.

Magnetic properties

The magnetochemical description of **1** and **2** using low-field susceptibility data is based on the phenomenological molecular-field approach due to the presence of a multitude of possible distinct exchange pathways as well as the different local coordination environments. In addition, the already published magnetic susceptibility data [2] of $Co(NCNH_2)_4Cl_2$, **3**, and $Ni(NCNH_2)_4Cl_2$, **4**, were reinvestigated for a better comparison.

On the basis of the electronic configuration of the Mn^{2+} ion ($3d^5$, free ion ^6S) in a distorted octahedral (i.e., tetragonal bipyramidal) coordination environment and, therefore, the existence of a resulting orbital singlet term $^6A_1$ for **2**, simple Curie-type spin magnetism (i.e., temperature independence of μ_{eff}) is expected if exchange interactions and saturation effects do not have a decisive influence. In all other cases, two factors cause the observed deviations from the scenario of Curie-type spin magnetism: first, orbital momentum contributions in the case of Cr^{2+}, Co^{2+}, and Ni^{2+} and, second, antiferromagnetic coupling between the magnetic ions within a given three-dimensional network for all compounds [14].

All the magnetic data were analyzed by using the program CONDON 2.0 [15] with the complete basis set as a function of the applied field ($\boldsymbol{B} = 0.1, 0.5$, and 1.0 T), which is necessary to yield reliable information on the magnetic dipole orientation with respect to the $D_{4\mathrm{h}}$ local symmetry of the metal ion. CONDON 2.0 takes into account the following single-ion effects: ligand-field effects (H_{lf}), interelectronic repulsion (H_{ee}), spin-orbit coupling (H_{so}), and the applied field (H_{mag}). Generally, for a magnetically isolated $3d^n$ metal ion in a ligand-field (lf) environment exposed to an external magnetic field $\boldsymbol{B}$, the Hamiltonian of the metal ion [16, 17] is represented by

$$H = H_{\mathrm{ee}} + H_{\mathrm{lf}} + H_{\mathrm{so}} + H_{\mathrm{ex}} + H_{\mathrm{mag}}.$$

This expression can be considered as an extension of the EHCF d-shell Hamiltonian [18] on account of the spin-orbit interaction operator H_{so} and the operator describing the interaction with the applied magnetic field H_{mag}. Fig. 4 shows the experimental magnetization (μ_{eff}, SI units; $\mu_{\mathrm{eff}} = 797.74\sqrt{\chi_{\mathrm{m}}T}$) of **1**, **2**, **3**, and **4** within the temperature range 2 – 290 K. This data set was fitted to the above-stated Hamiltonian using the ligand-field effect, spin-orbit coupling, and exchange coupling. The values for the spin-orbit coupling parameter and Racah parameters were chosen on the basis of the optical spectra and are consistent with our EHCF calculations [18].

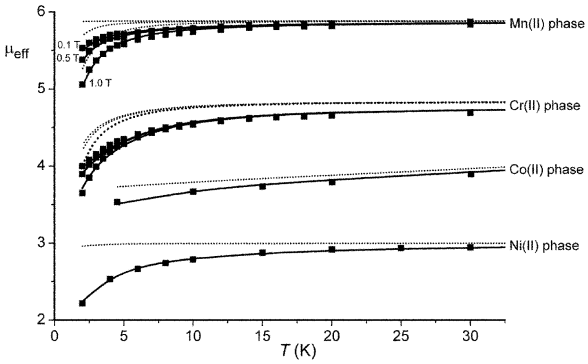

Fig. 4. Temperature dependence of μ_{eff} in μ_{B} of **1**, **2**, **3**, and **4** at applied fields of $B_0 = 0.1$, 0.5, 1 Tesla; see also text.

The exchange interactions between the metal ions are taken into account in the molecular field approximation

$$\chi_{\mathrm{m}}^{-1} = \chi_{\mathrm{m}}'^{-1}(B, C, \zeta, B_{\mathrm{q}}^{\mathrm{k}}) - \lambda_{\mathrm{mf}},$$

where $\chi_{\mathrm{m}}'^{-1}$ represents the single-center susceptibility and λ_{mf} the molecular-field parameter. The quantities $B_{\mathrm{q}}^{\mathrm{k}}$ represent the crystal/ligand-field parameters in Wybourne notation (B_0^2, B_0^4, and B_4^4 for a distorted octahedral coordination environment) according to

$$H_{\mathrm{lf}}^{\mathrm{tet}} = B_0^2 \sum_{i=1}^{N} C_0^2(i) + B_0^4 \sum_{i=1}^{N} C_0^4(i) + B_4^4 \sum_{i=1}^{N} \left(C_4^4(i) + C_{-4}^4(i)\right)$$

where $C_{\mathrm{q}}^{\mathrm{k}}(i)$ are the Racah tensor components describing the angular dependence of the ligand field. The B_q^k ligand-field parameters can be determined by the EHCF procedure [18].

At room temperature, the effective Bohr magneton number of **2** is roughly 5.9 per $Mn(NCNH_2)_4Cl_2$ unit or per high-spin Mn^{2+} ion, a value that corresponds to the spin-only value of 5.92 (see Fig. 4). The χ_{m}^{-1} *vs.* T plot reveals a linear behavior between 25 and 290 K.

This observation is supported by a linear fit of the reciprocal molar susceptibility to the Curie law above 25 K, leading to $C = 5.469 \times 10^{-5}$ m^3 K mol^{-1} with $\mu_{so} = 5.9\ \mu_B$ and a Weiss temperature $\theta = -0.3$ K.

An octahedral ligand field would generate, in the case of Ni^{2+}, an orbital singlet [**4**, $3d^8$, $^3A_2$; $\mu_{so} = 2.87\ \mu_B$], and an orbital doublet [**1**, $3d^4$, ^5E; $\mu_{so} = 4.90\ \mu_B$] ground state in the case of Cr^{2+}. The actual symmetry, however, is lower (C_{4v}) so that relative to this point group the symmetry notation changes to $^3B_1$ for Ni^{2+} whereas, for Cr^{2+}, the orbital doublet splits and the ground state is $^5B_1$. Therefore, Curie paramagnetism is observed if exchange interactions and saturation effects do not have a significant influence. The room temperature value depends on the ligand-field strength and the mixing of excited states into the ground term via spin-orbit interaction in both cases. In the range $T = 25-300$ K, the μ_{eff} values for Cr^{2+} ($\mu_{eff} = 4.74\ \mu_B$) and Ni^{2+} ($\mu_{eff} = 3.05\ \mu_B$) are independent of the temperature. The Curie-Weiss fit in the linear range of the χ_m^{-1} *vs.* T plot corresponds to $C = 3.5311 \times 10^{-5}$ m^3 K mol^{-1} and a Weiss temperature $\theta = -0.4$ K ($\mu_{so} = 4.74\ \mu_B$) for Cr^{2+}, whereas one finds $C = 1.4298 \times 10^{-5}$ m^3 K mol^{-1} and a Weiss temperature $\theta = -1.9$ K ($\mu_{so} = 3.05\ \mu_B$) for Ni^{2+}. There is no deviation from the spin-only values, but the small negative Weiss temperature manifests antiferromagnetic exchange interaction in the three-dimensional network.

The magnetic behavior of Co^{2+} [**3**, $3d^7$, $\mu_{so} = 3.87\ \mu_B$] is completely different from that of the other central ions. At room temperature, the effective Bohr magneton number (μ_{eff}) of 4.74 is significantly larger than the spin-only value because of the positive spin-orbit coupling term for ions after a half-filled 3*d* shell. There is no temperature-independent behavior in the μ_{eff} *vs.* T plot. The monotonous decrease of μ_{eff} towards lower temperatures for **3** is explained by single-ion effects (H_{lf}, H_{ee}, H_{so}) with a spatially degenerate ^4E ground state which results from the tetragonal deformation of the octahedral $^4T_1$ ground state.

For all four compounds, the fitting procedure employs starting values for the ligand-field parameters B_0^2, B_0^4, and B_4^4 that are directly picked from the EHCF calculations. The parameters used for Ni and Co in the EHCF calculations have been taken from the literature [24, 25], as was also done for Mn [26]; the hopping scaling parameters β^{ML} for $M =$ Cr and $L =$ N were also available [27]. Chlorine-containing compounds of Cr had not been calculated by the ECHF so far. Therefore, we estimated the hopping scaling parameter β^{ML} for $M =$ Cr and $L =$ Cl to be 1.70 in order to reproduce the fitted value of the B_0^2 parameter for **1**. The best fit results of the magnetic parameters are given in Table 2, in good agreement with the EHCF values and the molecular field parameter λ_{mf} indicating antiferromagnetic coupling. For the Co^{2+} complex the orbital reduction factor κ is equal to 0.75, nicely in line with data of Co complexes in the literature [28]. The ratios $B_2^2/B_0^2 = 0.53$ and $B_4^4/B_0^4 = 0.12$ were fixed at the values of the EHCF calculations.

Table 2. Results of the fitting procedures for the magnetic susceptibility data of 1–4.

Compound	Cr	Mn	Co	Ni
d^n	d^4	d^5	d^7	d^8
Free ion ground state	^5D	^6S	^4F	^3F
Ligand field (O_h) ground term	^5E	$^6A_1$	$^4T_1$	$^3A_2$
Ligand field (C_{4v}) ground term	$^5B_1$	$^6A_1$	^4E	$^3B_1$
No. of basis functions	210	252	120	45
B, ($C = 4B$), cm^{-1}	830	960	878	1080
ζ, cm^{-1}	230	347	533	649
C, 10^{-5} m^3 K mol^{-1}	3.5311	5.4691	–	1.4298
θ, K	−0.4	−0.3	–	−1.9
μ_{eff} at 290 K	4.74	5.91	4.78	3.05
B_0^2, cm^{-1} (EHCF)	1664	2128.9	1905.1	1592.9
B_0^4, cm^{-1} (EHCF)	28 438	15 036.6	15 656.2	19 447.8
B_4^4, cm^{-1} (EHCF)	18 134	9837.9	9897.5	12 348.4
B_0^2, cm^{-1}	2100	2100	4300	4750
B_0^4, cm^{-1}	24 050	15 100	18 200	39 100
B_4^4, cm^{-1}	15 800	9700	5400	23370
λ_{mf}, 10^4 mol m^{-3}	−1.064	−0.415	−2.713	−9.904
SQ, %[a]	0.9	0.7	0.8	0.5

[a] Quality of the fit: $SQ = (FQ/n)^{1/2} \times 100\,\%$, where $FQ = \sum_{i=1}^{n} \{[\chi_{obs}(i) - \chi_{cal}(i)]/\chi_{obs}(i)\}^2$.

The dotted lines in Fig. 4 illustrate the temperature dependence of μ_{eff} exclusively in terms of isolated single-ion and magnetic saturation effects, that is, in the complete absence of antiferromagnetic (AF) exchange coupling. Including AF interactions, the ligand-field overall splitting derived from this magnetochemical analysis corresponds well to spectroscopic data [19] on tetragonally distorted octahedral M^{2+} ($M =$ Cr, Mn, Co, Ni) complexes and is in line with our EHCF calculations. The symmetries and spins for the tetragonal (C_{4v}) group are also given in Table 2. The EHCF calculations for all four elements exhibit the splitting pattern of the *d* levels as shown in Scheme 1:

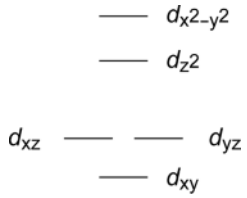

Scheme 1.

with $\varepsilon(xy) - \varepsilon(xz) < 0$ for the calculated values of the effective crystal fields, which fully explains the observed magnetic behavior.

According to our EHCF calculation, the d^7 (Co) compound **3** in the high-spin state is a Jahn-Teller system for which one may expect a deformation lifting the degeneracy of the ground electronic state. It has been shown [29] that in an analogous series of the $M(H_2O)_4Cl_2$ compounds this very Jahn-Teller distortion does take place in the Co member of the series. Such behavior, however, is not found for the present cyanamide series, probably due to the stiffer network involving hydrogen bonds between quasi-molecular moieties.

Experimental Section

Syntheses

Single crystals of $Mn(NCNH_2)_4Cl_2$ were prepared by dissolving 1 mmol (161.87 g mol^{-1}) $MnCl_2 \cdot 2H_2O$ and 4 mmol (42.04 g mol^{-1}) H_2NCN in 10 mL distilled water. After very slow evaporation of the aqueous solution under normal atmosphere within a few weeks, colorless cubic crystals were obtained.

Powderous $Cr(NCNH_2)_4Cl_2$, **1**, and $Mn(NCNH_2)_4Cl_2$, **2**, were prepared by treating anhydrous MCl_2 (M = Cr or Mn) and H_2NCN mixed in 1 : 4 ratio using an agate mortar at room temperature in a glove box. While the $Cr(NCNH_2)_4Cl_2$ powder is light blue, the $Mn(NCNH_2)_4Cl_2$ powder is pale pink. Both of them are sensitive to hydrolysis.

X-Ray structure determination

A colorless crystal of **2** was selected and mounted in a glass capillary with oil. The diffraction data were collected on an Bruker SMART APEX CCD area detector diffractometer with graphite-monochromatized MoK_α radiation. The structure is isotypic with $M(NCNH_2)_4Cl_2$ (M = Fe, Co, Ni and Cu) and was refined by full-matrix least-squares on F^2 using the SHELXL97 program [20]. As found before, N2 is distributed over two equal sites with 50 % occupancy [2], a result of the pyramidal configuration of the N2 atom. The position of the hydrogen atoms was found from a difference Fourier map. Details about the crystal data and data collection are summarized in Table 3. Tables 4 and 5 give positional and isotropic as well as anisotropic displacement parameters.

The structural characterization of powderous **1** was carried out at room temperature using a Stoe STADI MP diffractometer in transmission geometry with strictly monochromatized Cu$K_{\alpha 1}$ radiation and a linear position-sensitive detector (PSD) with a flat-sample holder; the range of measure-

Table 3. Crystal structure data for $Mn(NCNH_2)_4Cl_2$.

Formula; molar mass, g mol^{-1}	$Mn(NCNH_2)_4Cl_2$; 294.01
Crystal color and form	transparent block
Lattice parameter a, Å	12.8210(11)
Cell volume, Å^3	2107.5(3)
Space group; formula unit	$Im\bar{3}m$ (no. 229); 6
X-Ray density, g cm^{-3}; $F(000)$, e	1.39; 882
Instrument; radiation; λ, Å	Bruker SMART APEX CCD Area Detector, MoK_α, graphite monochromator; 0.71073
Temperature	273(2)
Reflections collected / unique	10146 / 545
Octants; max. 2θ, deg	$-17 \le h \le 16$, $-17 \le k \le 17$, $-17 \le l \le 17$; 58.42
Absorption correction	multi-scan
Absorption coefficient, mm^{-1}	1.3
Min. / max. transmission / R_{int}/R_σ	0.564 / 0.925 / 0.0363 / 0.0116
Structure solution	Isotypism with $M(NCNH_2)_4Cl_2$ (M = Fe, Co, Ni, Cu)
Structure refinement	Least-squares methods on F^2, Full matrix
No. of intensities, variables	321, 23
Weighting scheme	$w = [\sigma^2(F_o^2) + (0.044 \times P)^2 + 0.5717 \times P]^{-1}$, where $P = (\mathrm{Max}(F_o^2, 0) + 2F_c^2)/3$
Goodness of fit (all data)	1.193
Final R_1 / wR_2 indices $[I > 4\sigma(I)]$	0.0280 / 0.0828
Final R_1 / wR_2 indices (all data)	0.0318 / 0.0875
Max. / min. residual electron density, e Å^{-3}	0.38/−0.11

Atom	Wyckoff position	SOF	x	y	z	U_{eq}
Mn	6*b*	1	0	1/2	0	0.0610(3)
Cl	12*e*	1	0	0.29814(11)	0	0.0724(4)
N1	24*h*	1	0.37866(14)	0	0.37866(14)	0.0800(8)
C	24*h*	1	0.31720(18)	0	0.31720(18)	0.0696(8)
N2	48*k*	0.5	0.2459(2)	0.0263(8)	0.2459(2)	0.091(4)
H	48*j*	1	0.186(2)	0	0.2633(18)	0.086(9)

Table 4. Positional and isotropic displacement parameters (Å^2) for $Mn(NCNH_2)_4Cl_2$ with standard deviations in parentheses.

Atom	U_{11}	U_{22}	U_{33}	U_{23}	U_{13}	U_{12}
Mn	0.0476(3)	0.0877(7)	U_{11}	0	0.00000	0
Cl	0.0659(4)	0.0854(8)	U_{11}	0	0.00000	0
N1	0.0590(9)	0.122(3)	U_{11}	0	−0.0078(12)	0
C	0.0528(9)	0.103(2)	U_{11}	0	0.0041(12)	0
N2	0.0578(11)	0.157(12)	U_{11}	0.0062(18)	−0.0055(14)	U_{23}

Table 5. Anisotropic displacement parameters (Å^2) for $Mn(NCNH_2)_4Cl_2$ with standard deviations in parentheses.

Formula; molar mass, g mol^{-1}	$Cr(NCNH_2)_4Cl_2$; 291.06
Crystal color and form	light-blue powder
Lattice parameter a, Å	12.643(2)
Cell volume, Å^3	2021.0(4)
Space group; Z	$Im\bar{3}m$ (no. 229); 6
Number of reflections	149
R_p / R_{wp} / R_{Bragg}	0.028 / 0.038 / 0.082
2θ range, deg	5–105
Radiation; λ, Å	monochromatized CuK_{α_1}; 1.54059
Goodness of fit	1.45

Table 6. Crystallographic data for $Cr(NCNH_2)_4Cl_2$.

Atom	Wyckoff position	SOF	x	y	z	U_{eq}
Cr	6*b*	1	0	1/2	0	0.053(2)
Cl	12*e*	1	0	0.2829(3)	0	0.044(2)
N1	24*h*	1	0.3845(8)	0	0.3845(8)	0.064(5)
C	24*h*	1	0.3233(8)	0	0.3233(8)	0.049(7)
N2	48*k*	0.5	0.2511(5)	0.029(2)	0.2511(5)	0.059(10)

Table 7. Positional and isotropic displacement parameters (Å^2) for $Cr(NCNH_2)_4Cl_2$ with standard deviations in parentheses.

ment was 5 – 105° in 2θ with individual steps of 0.01°. The Rietveld method with a pseudo-Voigt profile and the FULLPROF program package [21] were used to perform structural refinement. The background of the data set was manually subtracted by linear interpolation. Because the hydrogen positions cannot be determined from powder X-ray diffraction data, their positions were for simplicity assumed to be the same as those of $Mn(NCNH_2)_4Cl_2$. The crystallographic data of $Cr(NCNH_2)_4Cl_2$ are shown in Table 6, atom positions and isotropic displacement parameters are listed in Table 7.

Further details of the crystal structure investigation may be obtained from Fachinformationszentrum Karlsruhe, 76344 Eggenstein-Leopoldshafen, Germany (fax: +49-7247-808-666; E-mail: crysdata@fiz-karlsruhe.de, http://www.fiz-karlsruhe.de/request_for_deposited_data.html) on quoting the deposition number CSD-424582 for $Cr(NCNH_2)_4Cl_2$ and CSD-424583 for $Mn(NCNH_2)_4Cl_2$.

Magnetic measurements

The temperature-dependent magnetic susceptibilities of **1** and **2** were determined by SQUID magnetometry (Quantum Design MPMS 5XL) between 2 and 300 K in applied fields of 0.1, 0.5 and 1.0 Tesla. The corresponding data of **3** and **4** were taken from a previous publication [2]. All data were corrected for the sample holder (PTFE capsules), and for diamagnetic contributions of the metal ions (Cr^{2+}, Mn^{2+}, Co^{2+}, and Ni^{2+}) and the ligands, calculated from tabulated values; $\chi_m^{dia} = -119 \times 10^{-11}$ m^3 mol^{-1} [22, 23].

Acknowledgement

It is a pleasure to thank Dr. Y. Wang for the single-crystal measurements. The financial support by the Deutsche Forschungsgemeinschaft is gratefully acknowledged, as is that from RFBR as dispatched to ALT through the grant no. 10-03-00155.

[1] O. Reckeweg, R. Dronskowski, T. Schleid, *Z. Kristallogr. NCS* **2008**, *223*, 221.

[2] X. Liu, P. Kroll, R. Dronskowski, *Z. Anorg. Allg. Chem.* **2001**, *627*, 1682 – 1686.

[3] X. Liu, R. Dronskowski, *Z. Kristallogr. NCS* **2002**, *217*, 118.

[4] H. G. von Schnering, B.-H. Brand, *Z. Anorg. Allg. Chem.* **1973**, *402*, 159 – 168.

[5] A. Zalkin, J. D. Forrester, D. H. Templeton, *Inorg. Chem.* **1964**, *3*, 529 – 533.

[6] B. R. Penfold, J. A. Grigor, *Acta Crystallogr.* **1959**, *12*, 850 – 854.

[7] K. Waizumi, H. Masuda, H. Ohtaki, K. Tsukamoto, I. Sunagawa, *Bull. Chem. Soc. Jpn.* **1990**, *63*, 3426 – 3433.

[8] K. Waizumi, H. Masuda, *Inorg. Chim. Acta* **1992**, *192*, 173 – 181.

[9] R. Eßmann, G. Kreiner, A. Niemann, D. Rechenbach, A. Schmieding, Th. Sichla, U. Zachwieja, H. Jacobs, *Z. Anorg. Allg. Chem.* **1996**, *622*, 1161 – 1166.

[10] J. D. Ternero, F. Fayos, *Z. Kristallogr.* **1990**, *192*, 147 – 148.

[11] R. D. Shannon, *Acta Crystallogr.* **1976**, *A32*, 751 – 767.

[12] J. W. Tracy, N. W. Gregory, E. C. Lingafelter, J. D. Dunitz, H.-C. Mez, R. E. Rundle, C. Scheringer, H. L. Yakel, Jr., M. K. Wilkinson, *Acta Crystallogr.* **1961**, *14*, 927 – 929.

[13] L. Denner, P. Luger, J. Buschmann, *Acta Crystallogr.* **1988**, *C44*, 1979 – 1981.

[14] F. E. Mabbs, D. J. Machin, *Magnetism and Transition Metal Complexes*, Chapman and Hall, London **1973**.

[15] M. Speldrich, H. Schilder, H. Lueken, P. Kögerler, *Isr. J. Chem.* **2011**, *51*, 215 – 227.

[16] B. G. Wybourne, *Spectroscopic Properties of Rare Earths*, Wiley, New York, London, Sydney **1965**.

[17] C. Görller-Walrand, K. Binnemans in *Handbook on the Physics and Chemistry of Rare Earths,* Vol. 23 (Eds.: J. K. A. Gschneidner, L. Eyring), Elsevier, Amsterdam **1996**, pp. 121.

[18] A. V. Soudackov, A. L. Tchougréeff, I. A. Misurkin, *Theor. Chim. Acta* **1992**, *83*, 389 – 416.

[19] A. B. P. Lever, *Inorganic Electronic Spectroscopy*, Elsevier, Amsterdam **1984**.

[20] G. M. Sheldrick, *Acta Crystallogr.* **2008**, *A64*, 112 – 122.

[21] J. Rodriguez-Carvajal, FULLPROF2000 (Version 3.2), A Program for Rietveld Refinement and Pattern Matching Analysis, Laboratoire Léon Brillouin (CEA-CNRS), Centre d'Etudes de Saclay, Gif sur Yvette (France) **1997**.

[22] W. Haberditzl, *Angew. Chem., Int. Ed. Engl.* **1966**, *5*, 288 – 298.

[23] H. Lueken, *Magnetochemie*, Teubner, Stuttgart **1999**, chapter 2.2, p. 40.

[24] A. V. Soudackov, A. L. Tchougréeff, I. A. Misurkin, *Zh. Fiz. Khim.* **1994**, *68*, 1256 – 1264 [in Russian]; *Russ. J. Phys. Chem.* **1994**, *68*, 1135 [in English].

[25] A. V. Soudackov, A. L. Tchougréeff, I. A. Misurkin, *Zh. Fiz. Khim.* **1994**, *68,* 1264 – 1270 [in Russian]; *Russ. J. Phys. Chem.* **1994**, *68*, 1142 [in English].

[26] A. M. Tokmachev, A. L. Tchougréeff, *Khim. Fiz.* **1999**, *18*, 80 – 87 [in Russian]; *Chem. Phys. Reports* **1999**, *18*, 163 [in English].

[27] A. L. Tchougréeff, *arXiv*: 1112.1362.

[28] B. N. Figgis, M. Gerloch, J. Lewis, F. E. Mabbs, G. A. Webb, *J. Chem. Soc. A: Inorganic, Physical, Theoretical* **1968**, 2086 – 2093.

[29] A. V. Soudackov, A. L. Tchougréeff, I. A. Misurkin, *Int. J. Quant. Chem.* **1996**, *57*, 663 – 671.